Preprints of the 21st IFAC World Congress (Virtual)
Berlin, Germany, July 12-17, 2020

Coordinated AFS and DYC for autonomous vehicle steerability and stability enhancement

Faïza KHELLADI, Rodolfo ORJUELA, Michel BASSET

Institut de Recherche en Informatique, Mathématiques, Automatique et Signal (IRIMAS EA 7499), 12 rue des Frères Lumière
F-68093 Mulhouse Cedex, France.
e-mail: (faiza-enfel.khelladi, rodolfo.orjuela, michel.basset)@uha.fr

Abstract. In this paper, the hierarchical yaw stability control architecture is introduced. This approach coordinates two controllers, namely the steerability and the stability controllers improving respectively the handling performance and the lateral stability. Thus, each controller has a control domain, a control objective, and its own active system. The coordination of these controllers is made by means of a supervisor that gives activation functions to prioritize each controller according to the detected situation whether it is critical or not. Using the same controllers, two supervisors are investigated. On one hand, the sideslip angle - sideslip rate phase plan, and the simplified yaw rate - sideslip angle phase plan on the other hand. Finally, simulation results are given to show the effectiveness of the proposed approach.

Keywords: Hierarchical approach, active front steering (AFS), Direct yaw control (DYC), coordinated control, stability criteria, Super-Twisting algorithm, control allocation.

1. INTRODUCTION

Vehicle safety is a major issue for industry as well as academia. However, despite of the given efforts, the vehicle performance improvement in terms of steerability and stability by developing an optimal yaw stability control (YSC) remains an open issue. The YSC regroups two main tasks, namely the steerability and the stability tasks as shown in Fig. 1. In detail, the steerability controller improves both handling performance and vehicle yaw stability for steady state driving conditions (linear domain). While, the stability controller is only used during critical driving conditions (non-linear domain) to improve the vehicle lateral stability [He, 2005, Doumiati et al., 2013, Aripin et al., 2014, Mousavinejad et al., 2017].

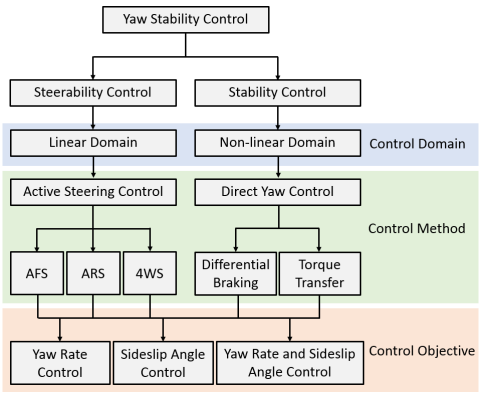

Figure 1. Yaw stability control

Several approaches are investigated to deal with the steerability task e.g. the active front steering (AFS) [He, 2005, Aripin et al., 2014], the active rear steering (ARS)[He, 2005], and the four wheel steering (4WS) [Aripin et al., 2014]. As mentioned in [He, 2005], the AFS is more effective than the ARS to maintain the vehicle stability near the handling limit at high speed. It is also a standard equipment for the current commercialized vehicles. For these reasons, the steerability is ensured here by an AFS. For the stability controller, the direct yaw control (DYC) using the differential braking is used here due to its effectiveness on highly extreme driving situations comparing to the torque transfer [Attia et al., 2014]. Given that the two controllers operate in different operating domains (linear and nonlinear domains) and that their control objectives are conflicting in some cases, the transition between these controllers seems to be crucial to determine the optimal nature of their coordination.

The transition between the two controllers is dictated by a supervisor detecting the lateral instability of the vehicle and activates the appropriate controller in every situation. This detection is based on the definition of a stable region wherein the steerability controller is prioritized. When the vehicle behavior becomes unstable while exceeding the stability boundaries, the stability controller would have the priority. Many stability criteria are proposed in the literature to define these boundaries. Among them, the sideslip angle - sideslip rate phase plan remains the most used [Doumiati et al., 2013, Mousavinejad et al., 2017, Termous et al., 2019, Chokor et al., 2019]. Other studies rely on the limitations of the yaw motion variables, namely the yaw rate and the sideslip angle as proposed in [Rajamani, 2012, Tondel and Johansen, 2005, Zhu et al., 2014]. Another phase plan technique based on the yaw

motion variables can be found in the literature under the name of yaw rate - sideslip angle phase plan. This phase plan does not tightly adhere to the phase plan concept but is still representative of the vehicle handling behavior as stated in [Mammar and Koenig, 2002]. This method is less investigated due to the complexity of determining the boundaries of the stability region [Liu et al., 2017]. Recently in [Khelladi et al., 2019], the effectiveness of this phase plan is improved through the decomposition made by considering the yaw motion limitations. This decomposition can then be used as supervisor to manage the AFS and the DYC in an integrated way.

The main contribution of this paper is the proposition of a hierarchical approach coordinating AFS and DYC based on the yaw rate - sideslip angle phase plan decomposition. In fact, this phase plan is decomposed in different operating regions. According to the phase trajectory through the regions, the contribution of each control action is taken into account by means of activation functions. The latter are employed by the controller layer ensuring the steerability as well as the lateral stability. Both controllers are based on a Super-Twisting approach [Termous et al., 2019] allowing to cope with model uncertainties and disturbance rejection. The proposed control strategy performance is then compared to that stemming from a similar architecture based this time on the classic sideslip angle - sideslip rate phase plan used as a supervisor. The proposed approach offers a control energy reduction to guarantee the lateral stability and thus the breaks are less solicited.

This paper is structured as follows: Section 2 introduces the vehicle model. The lateral stability analysis based on each phase plan is presented in Section 3. Section 4 is dedicated to the presentation of the global hierarchical control architecture with the description of each part of it. The simulation results supporting the comparison made are discussed in Section 5.

2. VEHICLE MODEL

The whole control architecture is based on the 6-DOF model [Rajamani, 2012] presented in this section. The lateral velocity V_y and the yaw rate $\dot{\psi}$ constitute two degrees of freedom while the other four degrees of freedom are the wheel velocities ω_i.

Vehicle dynamics equations. The vehicle's lateral and yaw motions are respectively defined by

$$\begin{aligned} m\dot{V_y} &= F_{yrl} + F_{yrr} + (F_{xfl} + F_{xfr})sin(\delta) \\ &\quad + (F_{yfl} + F_{yfr})cos(\delta) - m\dot{\psi}V_x \end{aligned} \tag{1a}$$

$$\begin{aligned} I_z\ddot{\psi} &= L_f(F_{yfl} + F_{yfr})cos(\delta) - L_r(F_{yrl} + F_{yrr}) \\ &\quad + \frac{L_w}{2}(F_{yfl} - F_{yfr})sin(\delta) + M_z \end{aligned} \tag{1b}$$

where F_{xi} and F_{yi} ($i \in \{fl, fr, rl, rr\}$) are respectively the longitudinal and lateral tire forces at front left, front right, rear left, and rear right. V_x is the longitudinal velocity, δ is the steering angle, m is the vehicle total mass, L_f and L_r are respectively the front and the rear center of gravity (CoG) distances, L_w is the track width, I_z is the vehicle moment of inertia around the vertical axis. The stabilizing yaw moment M_z is defined as

$$\begin{aligned} M_z = \; & L_f(F_{xfl} + F_{xfr})sin(\delta) + \tfrac{L_w}{2}(F_{xfr} - F_{xfl})cos(\delta) \\ & + \tfrac{L_w}{2}(F_{xrr} - F_{xrl}) \end{aligned} \tag{2}$$

Wheel dynamics equations. The following equation of torque balance is valid for each wheel,

$$J_\omega\dot{\omega}_i = T_{d_i} - T_{b_i} - rF_{xi} \tag{3}$$

where T_{d_i}, and T_{b_i} are respectively the driving and the braking torques, r the wheel effective rolling radius and J_ω the wheel moment of inertia.

A linear 2-DOF vehicle model considering assumptions mentioned in Rajamani [2012] is considered. Hence, the lateral model represented by (1) can be rewritten in a state-space formulation as

$$\dot{x} = Ax + B_1M_z + B_2\delta, \quad y = Cx \tag{4}$$

where: $A = \begin{bmatrix} -\frac{2(C_{\alpha_f}+C_{\alpha_r})}{mV_x} & -\frac{2(C_{\alpha_f}L_f - C_{\alpha_r}L_r)}{mV_x^2} - 1 \\ -\frac{2(C_{\alpha_f}L_f - C_{\alpha_r}L_r)}{I_z} & -\frac{2(C_{\alpha_f}L_f^2 + C_{\alpha_r}L_r^2)}{I_zV_x} \end{bmatrix}$

$B_1 = \begin{bmatrix} 0 \\ \frac{1}{I_z} \end{bmatrix}$, $B_2 = \begin{bmatrix} \frac{2C_{\alpha_f}}{mV_x} \\ \frac{2L_fC_{\alpha_f}}{I_z} \end{bmatrix}$, $C = \mathrm{I}$, $x = \begin{bmatrix} \beta \\ \dot{\psi} \end{bmatrix}$, $\beta \approx \frac{V_y}{V_x}$

The control inputs δ and M_z are respectively used for the steerability and the stability controllers described in Section 4. Both $\dot{\psi}$ and β are supposed measurable.

3. VEHICLE'S STABILITY ANALYSIS: STABILITY CRITERIA COMPARISON

Vehicle stability analysis is a significant step to subsequently design the YSC. Indeed, the latter is composed of the steerability and the stability controllers that may conflict with each other and are therefore prioritized according to the vehicle behavior [He, 2005].

The analysis of the vehicle stability is to define a stable region (linear domain) wherein the steerability controller is activated. During critical situations, the vehicle behavior becomes unstable and exceed the stability boundaries (non-linear domain). This situation requires the stability controller (Fig. 1).

3.1 Sideslip angle - sideslip rate phase plan

In this phase plan, the sideslip motion of the vehicle is bounded as shown in Fig.2. The stability index term (SI) is often associated to this phase plan approach:

$$SI = 2.49\dot{\beta} + 9.55\beta \tag{5a}$$

$$|\, SI \,| < 1 \tag{5b}$$

It represents a set of stable region boundaries as depicted in Fig. 2. Within these boundaries, the phase trajectories always converge to the stable value. However, when the phase trajectories are outside the boundaries and the sideslip angle and its derivative have the same sign, they are considered to be increasing and diverging from the stable value [Selby, 2003].

The narrower reference region for the stability control design (Fig. 2) is set in order to get a smooth transition

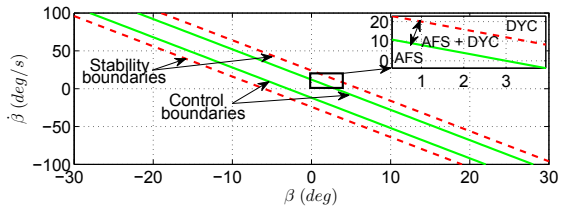

Figure 2. Sideslip angle - sideslip rate phase plan

between the steerability and the stability controllers as shown in Fig. 3 (see [Termous et al., 2019]). This new region implies early stability control action and thus more stable vehicle behavior [He, 2005].

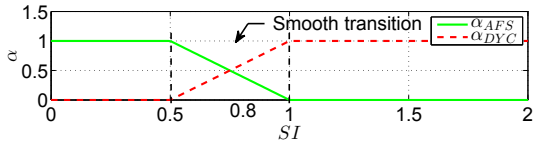

Figure 3. Controllers switching functions according to SI

α_{AFS} and α_{DYC} are activation functions for the AFS and the DYC respectively.

3.2 Yaw rate - sideslip angle phase plan

The simplified yaw rate - sideslip angle phase plan proposed in [Khelladi et al., 2019] is used here. This phase plan is based on the yaw motion variables limitations introduced in [Rajamani, 2012]:

$$\dot{\psi}_{max} = 0.85\frac{\mu g}{V_x} \tag{6a}$$

$$\beta_{max} = tan^{-1}(0.02\mu g) \tag{6b}$$

It can be noticed that the stability region is largely influenced by the vehicle speed V_x and the road adhesion coefficient μ. Thus, the phase plan is decomposed as shown in Fig. 4. The unstable region is defined as the case when the two variables exceed their limits at the same time which may be extremely dangerous provoking an oversteering situation [Nielsen and Kiencke, 2000].

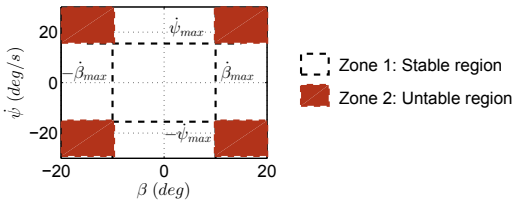

Figure 4. Yaw rate - sideslip angle phase plan

The transition between the two regions and thus between the stability and the steerability controllers is presented in Section 4.

4. HIERARCHICAL COORDINATED CONTROL ARCHITECTURE

The proposed control architecture for the YSC is a hierarchical structure composed of three levels as pictured in Fig. 5.

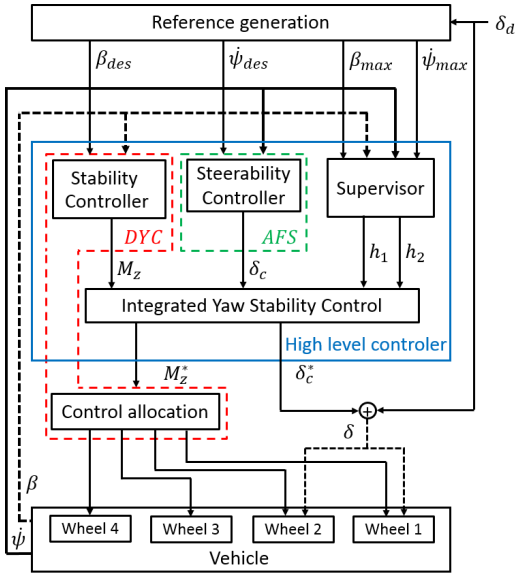

Figure 5. Yaw stability control architecture

The reference generation level provides the desired yaw motion variables $\dot{\psi}_{des}$ and β_{des} and their limitations $\dot{\psi}_{max}$ and β_{max} according to the vehicle speed V_x and the road adhesion coefficient μ. The reference variables tracking is obtained by a YSC at a high level controller shown in Fig.5. The latter is composed of a steerability controller that gives the appropriate corrective steering angle δ_c during normal driving situations on one hand, and a stability controller providing the needed stabilizing yaw moment M_z to stabilize the vehicle during critical situations on the other hand. The smooth transition between these two controllers is handled by a supervisor that detects critical situations and subsequently prioritizes the stability controller. Finally, the hierarchy's lowest level is meant to allocate the control command M_z^* to the multiple wheel brakes providing thus the differential braking. Each level is developed separately in this section.

4.1 Supervisor design

The supervisor used depends on the yaw rate - sideslip angle phase plan decomposition shown in Fig. 4. The goal of this decomposition is to exploit the steerability controller in zone 1 (stable region) as long as its effectiveness is guaranteed and whose control objective is the yaw rate. The second zone (unstable region) defines critical situations [Nielsen and Kiencke, 2000] that are handled by the stability controller. Its control objective is the sideslip angle. For the supervisor design, the centers chosen for each zone according to (6) are given by

$$\begin{bmatrix} C_{\dot{\psi}} \\ C_{\beta} \end{bmatrix} = [C_{h_1} \; C_{h_2}] \tag{7}$$

where:

$$C_{h_1} = \begin{bmatrix} 0 & -\dot{\psi}_{max} & \dot{\psi}_{max} & 0 & 0 \\ 0 & 0 & 0 & -\beta_{max} & \beta_{max} \end{bmatrix}$$

$$C_{h_2} = \begin{bmatrix} -\dot{\psi}_{max} & -\dot{\psi}_{max} & \dot{\psi}_{max} & \dot{\psi}_{max} \\ -\beta_{max} & \beta_{max} & -\beta_{max} & \beta_{max} \end{bmatrix}$$

These centers are used to compute the activation functions through the following expression

$$H_j(\xi) = \frac{\eta_j(\xi)}{\sum_{j=1}^{L} \eta_j(\xi)} \tag{8}$$

where, η_j is expressed by

$$\eta_j(\xi) = \prod_{j=1}^{L} exp\left(-\frac{(\xi - C_j)^T(\xi - C_j)}{\sigma^2}\right) \tag{9}$$

with $\xi = [\dot{\psi}\ \beta]^T$ the decision variables vector, L the number of centers ($L = 9$) and C_j the j column of the centers defined by (7). The shape parameter σ is a significant parameter to determine the nature of the transition between the zones. The larger σ the smoother the transition. The activation functions (8) are grouped in a way to get an activation function per zone as follows

$$\begin{cases} h_1(\xi) = \sum_{j=1}^{5} H_j(\xi) \\ h_2(\xi) = \sum_{j=6}^{9} H_j(\xi) \end{cases} \tag{10}$$

where h_1 indicates the activation of the AFS and h_2 the activation of the DYC.

4.2 Steerability and stability controllers design

Super-Twisting algorithm. The Super-Twisting algorithm is widely used in the automotive context [Mousavinejad et al., 2017], [Termous et al., 2019], [Chokor et al., 2019] due to its advantages like the robustness to parameter uncertainties and disturbances, and also the attenuation of the chattering phenomenon. The principle of this controller is to generate a continuous control law to restrict the system trajectories to reach in a finite time a sliding surface and remain on it. By considering the system below

$$\dot{x} = f(x,t) + g(x,t)u \tag{11}$$

with u and x the input and the state vectors, f and g continuous functions. The sliding surface S is defined with a relative degree of one with respect to u, and its derivative is written in the following form [Termous et al., 2019]:

$$\dot{S}(S,t) = \Phi(S,t) + \phi(S,t)u \tag{12}$$

It is assumed that positive constants C_0, b_{min}, b_{max} exist and satisfy the following conditions

$$\begin{cases} \mid \Phi(S,t) \mid < C_0 \\ 0 < b_{min} \leq \mid \phi(S,t) \mid \leq b_{max} \end{cases} \tag{13}$$

The Super-Twisting control law is finally given by:

$$u_c = u_1 + u_2 \begin{cases} u_1 = -\alpha_1 \mid S \mid^{0.5} sign(S) \\ \dot{u}_2 = -\alpha_2 sign(S) \end{cases} \tag{14}$$

where α_1 and α_2 are positive constants defined by

$$\begin{cases} \alpha_1 \geqslant \sqrt{\frac{4C_0(b_{max}\alpha_2 + C_0)}{b_{min}^2(b_{min}\alpha_2 - C_0)}} \\ \alpha_2 > \frac{C_0}{b_{min}} \end{cases} \tag{15}$$

and satisfying conditions of the finite time convergence to the sliding surface. This control approach is used for both the stability and the steerability controllers design.

Steerability controller design (AFS controller). The AFS controller is used during steady state driving conditions to improve the vehicle steerability. It provides the additive correction steering angle δ_c that adjusts the driver steering angle δ_d while the moment M_z is considered as an exogenous input here. Its control objective is to make the vehicle yaw rate $\dot{\psi}$ converging to the desired one $\dot{\psi}_{des}$ expressed by

$$\dot{\psi}_{des} = \frac{V_x}{L_f + L_r + \frac{mV_x^2(L_rC_{\alpha_r} - L_fC_{\alpha_f})}{2C_{\alpha_f}C_{\alpha_r}(L_f + L_r)}}\delta \tag{16}$$

It is formulated by considering the steady state yaw rate ($\ddot{\psi} = 0$ (4)). Let us remark that $\dot{\psi}_{des}$ is bounded by the yaw rate limitation expressed with (6a) i.e.

$$\mid \dot{\psi}_{des} \mid \leq \dot{\psi}_{max} \tag{17}$$

because of the road adhesion coefficient that does not allow to provide the necessary tire forces supporting a high yaw rate [Rajamani, 2012].

For the yaw rate tracking, the following sliding surface is chosen

$$S_1 = \dot{\psi} - \dot{\psi}_{des} \tag{18}$$

It can be noticed that S_1 has a relative degree of 1 with respect to δ (see (4)) and its derivative can be written in the form (12) that also satisfies the conditions (13). The Super-Twisting control law satisfying the yaw rate tracking is given by:

$$\delta_c = \delta_1 + \delta_2 \begin{cases} \delta_1 = -\alpha_{1_{\dot{\psi}}} \mid S_1 \mid^{0.5} sign(S_1) \\ \dot{\delta}_2 = -\alpha_{2_{\dot{\psi}}} sign(S_1) \end{cases} \tag{19}$$

with $\alpha_{1_{\dot{\psi}}}$ and $\alpha_{2_{\dot{\psi}}}$ are positive constants that satisfy conditions (15). The corrective steering angle δ_c will be applied according to the activation function h_1 as shown in Fig. 5, hence,

$$\delta_c^* = h_1\delta_c \tag{20}$$

Stability controller design (DYC controller). The DYC is only activated in critical situations to improve the vehicle stability when the front tires are saturated making the AFS no longer effective. This controller provides a stabilizing yaw moment M_z in order to guarantee the control objective of maintaining the sideslip angle and its derivative as small as possible. The steering input δ is treated as an exogenous input here. The choice of $\dot{\psi}_{des}$ makes the sideslip angle asymptotically converges to zero

$$\dot{\beta} = -\lambda\beta \tag{21}$$

with $\lambda = \frac{C_{\alpha_f} + C_{\alpha_r}}{mV_x}$ and consequently, the following sliding surface is chosen

$$S_2 = \dot{\beta} + \lambda\beta \tag{22}$$

S_2 has a relative degree of 1 with respect to M_z so its derivative is written in the form (12) satisfying the conditions (13). Hnece, the Super-Twisting control law is:

$$M_z = M_{z_1} + M_{z_2} \begin{cases} M_{z_1} = -\alpha_{1_\beta} \mid S_2 \mid^{0.5} sign(S_2) \\ \dot{M}_{z_2} = -\alpha_{2_\beta} sign(S_2) \end{cases} \tag{23}$$

with α_{1_β} and α_{2_β} are positive constants that also satisfy conditions (15). Finally, the M_z will be applied according to the activation function h_2 as

$$M_z^* = h_2M_z \tag{24}$$

4.3 Control allocation design

The control allocation level is the lower level of the hierarchy that aims to physically generate the stabilizing yaw moment M_z^* (24). During critical situations, especially oversteering situations determined by h_2, it is more efficient to generate M_z^* by applying braking torques on the

outer wheels. From an optimal control allocation point of view, the use of only one wheel to generate M_z^* seems a relevant choice to reduce the differential braking effect on the longitudinal speed. Consequently, some studies favor the use of one rear wheel brake at a time to also avoid overlapping with front steering actuators [Doumiati et al., 2013], [Chokor et al., 2019]. However, being based on one wheel to generate M_z^*, the latter may not be delivered if that wheel is already saturated or defective.

Thus, in this study, M_z^* is generated by the four wheel brakes through an optimal control allocation, by considering a linear effector model to rewrite (2) as $M_z^* = BF_{x_a}$, with

$$B = [B_{fl}\ B_{fr}\ B_{rl}\ B_{rr}] \quad (25)$$

$$F_{x_a} = \left[F_{x_{fl_a}}\ F_{x_{fr_a}}\ F_{x_{rl_a}}\ F_{x_{rr_a}}\right]^T \quad (26)$$

where,

$B_{fl} = L_f sin(\delta_f) - \frac{L_w}{2} cos(\delta_f)$, $B_{rl} = -\frac{L_w}{2}$
$B_{fr} = L_f sin(\delta_f) + \frac{L_w}{2} cos(\delta_f)$, $B_{rr} = \frac{L_w}{2}$

The control allocation computes the longitudinal efforts F_{xi_a} applied thereafter on each wheel as a braking torque ($T_{bi} = rF_{xi_a}$). Consequently, the problem formulation is expressed as

$$F_{x_a} = \arg\min_{F_{x_a}} \|M_z^* - BF_{x_a} + s\| \quad (27)$$

with s the slack variable that ensures the feasability of the problem. The allocation problem (27) is solved by using a standard quadratic programming as in [Khelladi et al., 2019].

5. SIMULATION RESULTS

In this section, the performance of the proposed hierarchical control architecture for the YSC is investigated. The results are compared with those obtained from the same architecture with a different supervisor based this time on the sideslip angle - sideslip rate phase plan. Thus, for the comparison issue, the same sliding mode controllers are used, the difference lies in the activation functions. Hence, the activation functions h_1 (AFS) and h_2 (DYC) in (20) and (24) are replaced by α_{AFS} and α_{DYC} respectively. Throughout this section, the following notations are used:

- **Proposed approach:** the supervisor is based on the yaw rate - sideslip angle phase plan.
- **Classic approach:** the supervisor is based on the sideslip angle - sideslip rate phase plan.

The vehicle parameters of the Renault Scenic are used (Table 1) through the CarMaker environment.

Table 1: Vehicle parameters

I_z(kg^{2}m)	J_ω(kg^{2}m)	L_f(m)	L_r(m)	L_w(m)
3503	0.99	1.035	1.655	1.535
$C_{\alpha f}$(N.rad^{-1})	$C_{\alpha r}$(N.rad^{-1})	r(m)	m(kg)	V_x(km/h)
97035	91631	0.313	1828	100

5.1 Test description

In this study, the normalized double lane change test, known also as the elk test, is performed by considering a dry road ($\mu = 0.9$) with an initial vehicle speed of ($V_{x_{init}} = 100km/h$).

5.2 Test results

The controlled and uncontrolled yaw motion variables of the vehicle are pictured in Fig.6 and 7. Both approaches aim to better track the desired yaw rate and minimize the sideslip angle meaning that the control objectives are accomplished and consequently the lateral stability is ensured. In fact, the activation functions are tuned to get the same vehicle responses.

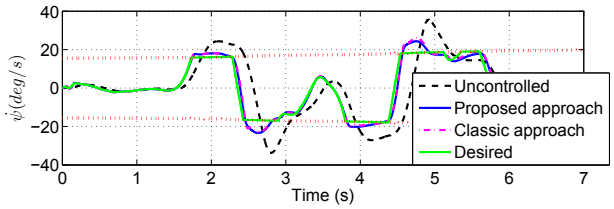

Figure 6. Yaw rate time response

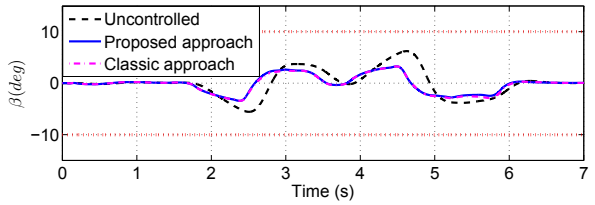

Figure 7. Sideslip angle time response

However, the main difference between these approaches lies in the coordination mechanism generating different control signals M_z and δ_c as depicted in Fig. 8 and 9.

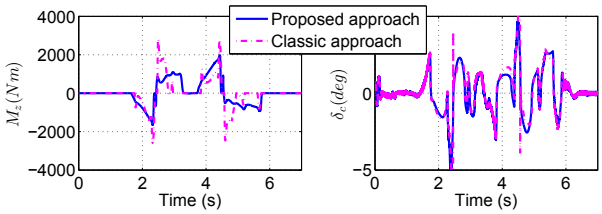

Figure 8. Yaw moment and corrective steering angle

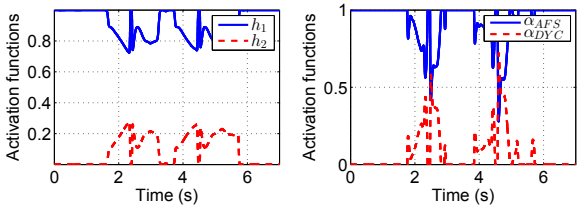

Figure 9. Comparison of activation functions

In Fig. 9, it can be noticed that before the first vehicle turn, h_1 and α_{AFS} (continuous lines) are at their maximum value of one indicating a stable behavior of the vehicle. During the double lane change (critical case), the activation function h_2 is smaller than α_{DYC}. This means that the DYC is less activated in the proposed approach

to stabilize the vehicle. Consequently, for similar closed-loop performance, δ_c coming from the AFS is similar for both approaches. However, M_z provided by the DYC is larger for the classic approach than the one obtained with the proposed approach (Fig. 8). The brakes are then less solicited in the proposed approach.

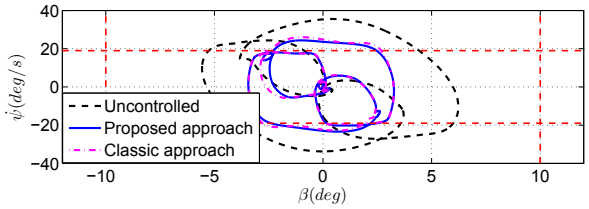

Figure 10. Yaw rate - sideslip angle phase plan

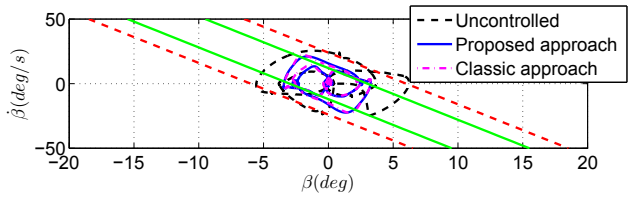

Figure 11. Sideslip angle - sideslip rate phase plan

According to Fig. 10, the proposed approach indicates a phase trajectory in zone 1 approaching zone 2 meaning that both AFS and DYC are coordinated ($h_2 \neq 0$) as pictured in Fig. 9. Similarly, Fig. 11 indicates that the phase trajectory in the classic approach still in the stability boundaries but slightly exceeds the control boundaries meaning that both controllers are coordinated ($\alpha_{DYC} \neq 0$). To summarize, the proposed approach is less energy demanding for lateral stability issue.

6. CONCLUSION

This paper presents an advanced YSC hierarchical architecture that coordinates the AFS and the DYC. In this architecture, a simplified yaw rate - sideslip angle phase plan decomposition is employed as a supervisor to coordinate the two controllers. The performance of the proposed architecture has been compared through simulations with those obtained from the same architecture with this time a supervisor based on the sideslip angle - sideslip rate phase plan. In both cases, the same Super-Twisting controllers are used. The comparison shows the effectiveness of the proposed architecture that reduces the control input energy in particular for stability task and thus solicits less the brakes.

This work could lead to consider the understeering situation by including additional information in zone 1 in order to use a second active system (active brakes) to better meet the driver's intention. The allocation level could also be based on the under/over-steering information in order to better exploit the tires ability of providing the necessary stabilizing brakes.

ACKNOWLEDGEMENTS

The authors gratefully acknowledge the financial support from the Alfred and Valentine Wallach foundation (France) for the SIMPHA project.

REFERENCES

M. K. Aripin, Y. Md Sam, K. A. Danapalasingam, N. Hamzah K. Peng, and M. F. Ismail. A Review of Active Yaw Control System for Vehicle Handling and Stability Enhancement. *International Journal of Vehicular Technology*, 2014:15, 2014.

R. Attia, R. Orjuela, and M. Basset. Dual-mode Control Allocation for Integrated Chassis Stabilization. In *19th IFAC WC*, Cape Town, South Africa, 2014.

A. Chokor, R. Talj, M. Doumiati, and A. Charara. A global chassis control system involving active suspensions, direct yaw control and active front steering. In *9th IFAC Symposium on Advances in Automotive Control*, Orléans, France, 2019.

M. Doumiati, O. Sename, L. Dugard, J.J. Martinez Molina, P. Gaspar, and Z. Szabo. Integrated vehicle dynamics control via coordination of active front steering and rear braking. *European Journal of Control*, 19(2):121–143, 2013.

J. He. *Integrated Vehicle Dynamics Control Using Active Steering, Driveline and Braking*. PhD thesis, The University of Leeds, School of Mechanical Engineering, 2005.

F. Khelladi, R. Orjuela, and M. Basset. Direct yaw control based on a phase plan decomposition for enhanced vehicle stability. In *10th IFAC Symposium on Intelligent Autonomous Vehicles*, Gdansk, Poland, 2019.

W. Liu, L. Xiong, B. Leng, H. Meng, and R. Zhang. Vehicle stability criterion research based on phase plane method. In *WCX 17: SAE WC*, Detroit, United States, 2017.

S. Mammar and D. Koenig. Vehicle handling improvement by active steering. *Vehicle System Dynamics*, 38(3):211–242, 2002.

E. Mousavinejad, Q. L. Han, F. Yang, Y. Zhu, and L. Vlacic. Integrated control of ground vehicles dynamics via advanced terminal sliding mode control. *Vehicle System Dynamics*, 55(2):268–294, 2017.

L. Nielsen and U. Kiencke. *Automotive Control Systems: For Engine, Driveline, and Vehicle*. Springer, 2nd edition, 2000.

R. Rajamani. *Vehicle dynamics and control*. Mechanical engineering series. Springer, 2nd edition, 2012.

M. A. Selby. *Intelligent Vehicle Motion Control*. PhD thesis, The University of Leeds, School of Mechanical Engineering, 2003.

H. Termous, H. Shraim, R. Talj, C. Francis, and A. Charara. Coordinated control strategies for active steering, differential braking and active suspension for vehicle stability, handling and safety improvement. *Vehicle System Dynamics*, 57(10):1494–1529, 2019.

P. Tondel and T.A. Johansen. Control allocation for yaw stabilization in automotive vehicles using multiparametric nonlinear programming. In *IEEE ACC*, Portland, OR, USA, 2005.

B. Zhu, Y. Chen, and J. Zhao. Integrated chassis control of active front steering and yaw stability control based on improved inverse nyquist array method. *Scientific World Journal*, 2014(2):14, 2014.